coatings

MDPI

Article

Wide-Range SPRi Sensors Based on Aptamer/sPD-L1/anti–PD-L1 Sandwich and AuNPs Enhancement for Ultrasensitive Detection of sPD-L1

Yuyan Peng [1], Li Jiang [2,*], Yifan Li [2] and Xiaoping Yu [1,*]

[1] School of Life Science, China Jiliang University, Hangzhou 310018, China; yuyanpeng423@163.com
[2] School of Optical and Electronic Technology, China Jiliang University, Hangzhou 310018, China; yifanli369@163.com
* Correspondence: lijiang@cjlu.edu.cn (L.J.); yxp@cjlu.edu.cn (X.Y.)

Abstract: Soluble programmed death-ligand 1 (sPD-L1) levels vary widely among different stages of tumor development, so the direct quantification of sPD-L1 as a cancer biomarker is useful in cancer diagnosis, prognosis and therapeutic assessment. There is an urgent need for an sPD-L1 detection method with a broad detection range and high sensitivity for monitoring cancer progression and evaluating the effectiveness of immunotherapy in real time. Herein, we have reported an enzyme-free, label-free surface plasmon resonance imaging (SPRi) sensor based on an aptamer/sPD-L1/anti–PD-L1 sandwich structure with gold nanoparticle (AuNP) signal enhancement for the ultrasensitive quantitative measurement of sPD-L1 for the first time. The gold chip of the SPRi sensing platform was modified by DNA aptamers, sPD-L1 was specifically adsorbed on the surface of a DNA aptamer-modified gold chip and then coupled with anti–PD-L1. Thus, the detection of sPD-L1 at different concentrations was realized through the formation of an aptamer/sPD-L1/anti–PD-L1 sandwich structure. We also enhanced the SPR signal via AuNPs to further improve sensor sensitivity. The SPRi sensor is able to measure sPD-L1 within a linear range of 50 pM–10 nM and 100 fM–50 pM, and the minimum detection limit is 19 fM. The sensor is designed to be widely applicable, with better accuracy and reliability for more application scenarios. The prepared SPRi sensor shows great potential in improving the sensitivity of detecting sPD-L1. The proposed method demonstrates the excellent performance of the SPRi sensor and provides a possibility for the establishment of effective clinical assay methods in the future.

Keywords: programmed death-ligand 1; surface sandwich assay; DNA aptamer/antibody bioreceptor pair; surface plasmon resonance; tumor biomarker

check for updates

Citation: Peng, Y.; Jiang, L.; Li, Y.; Yu, X. Wide-Range SPRi Sensors Based on Aptamer/sPD-L1/anti–PD-L1 Sandwich and AuNPs Enhancement for Ultrasensitive Detection of sPD-L1. *Coatings* **2023**, *13*, 1400. https://doi.org/10.3390/coatings13081400

Academic Editor: You Seung Rim

Received: 11 July 2023
Revised: 3 August 2023
Accepted: 8 August 2023
Published: 9 August 2023

Copyright: © 2023 by the authors. Licensee MDPI, Basel, Switzerland. This article is an open access article distributed under the terms and conditions of the Creative Commons Attribution (CC BY) license (https://creativecommons.org/licenses/by/4.0/).

1. Introduction

Programmed death-ligand 1 (PD-L1) is a co-regulatory molecule that is expressed on the surface of tumor cells. It interacts with its receptor programmed cell death 1 (PD-1) and is able to inhibit T-cell activity, thus allowing tumor cells to escape the body's autoimmunity to avoid death [1]. PD-L1 is commonly expressed on the surface of tumor cells, immune cells and other cells in the tumor microenvironment but is also present in extracellular forms, including in exosomes and microvesicles, as well as freely soluble forms of PD-L1 (sPD-L1) [2]. It has been shown that soluble PD-L1 levels are higher in cancer patients than in healthy controls [3–5], and higher levels of soluble PD-L1 are associated with poor prognosis in patients with solid tumors [6]; therefore, the detection of PD-L1 can be a useful indicator in early tumor diagnosis and prognosis prediction. However, there are still many difficulties in the detection of sPD-L1 at present. As a transmembrane protein, the level of sPD-L1 in the blood is low, and sPD-L1 is likely to reduce its natural activity when separated from the membrane environment due to its distinct hydrophobic structural domain [7].

Immunohistochemistry (IHC) is the main method used to detect PD-L1 in clinical practice. IHC is a classical method for detecting protein expression, which is evaluated via microscopic observation, according to the shade resulting from antibody staining [1]. Other methods used are the enzyme-linked immunosorbent assay (ELISA) [8] and electrochemistry [9], which are able to perform the accurate and sensitive detection of PD-L1 via novel antibodies or composites. However, the steps involved in ELISA are cumbersome and time consuming. Although the electrochemical method solves the above problems, it still needs to be improved in terms of sensitivity and multi-component analysis.

Surface plasmon resonance imaging (SPRi) is a label-free detection method based on SPR technology [10]. The mechanism of SPR technology is that a very small refractive index change at the interface of a metal medium affects the surface plasmon resonance effect excited by incident p-polarized light, resulting in a corresponding change in the reflectivity and phase of the reflected light, so that the reflectivity and phase of the reflected light can be determined. Based on this mechanism, SPR sensors have been applied to biomolecular interaction analysis, immunosensing, gas detection, etc. However, the lower detection limit of conventional SPR sensors is insufficient and, in order to solve this problem, precious metal nanoparticles, such as Au, which have stable chemical properties, are used due to the local surface plasmon resonance (LSPR) of the nanoparticles and the metal-sensitive films of the SPR are electromagnetically coupled to each other. The application of gold nanoparticles as sensing enhancers for signal amplification or sensitivity enhancement is a good option [11,12].

In this study, a relatively sensitive, real-time-monitoring SPR sensor based on gold nanoparticles was designed for the quantitative detection of soluble PD-L1. The specific aptamer and anti–PD-L1 were selected to target soluble PD-L1, and the dual recognition formed an aptamer/sPD-L1/anti–PD-L1 sandwich structure, enabling the specific quantitative detection of PD-L1. By coupling gold nanoparticles in advance to increase the local plasmon resonance and mass-loading effect, a simple signal amplification can achieve ultrahigh sensitivity, with the lowest detection limit reaching the fM level, which is an order of magnitude lower than previous studies. Moreover, the detection time is only 30 min, which greatly improves the detection efficiency. The results show that the constructed sensor has good feasibility and stability for the quantitative detection of sPD-L1 and has a very high sensitivity and low detection limit. The great potential of the sensor for clinical use was verified through serum-spiking experiments.

2. Materials and Methods

2.1. Materials

1-(3-Dimethylaminopropyl)-3-ethylcarbodiimide hydro (EDC, GE Healthcare Bio-Sciences AB, Machelen, Belgium), N-hydroxysulfosuccinimide (NHSS or sulfo-NHS, GE Healthcare Bio-Sciences AB, Belgium), 11-mercaptoundecanoic acid (MUA, Cool Seoul Bioengineering Co., Ltd., Hefei, China), 6-mercapto-1-hexanol (MCH, Shanghai Macklin Biochemical Co., Ltd., Shanghai, China), ascorbic acid (AA, Aladdin, Shanghai, China), plasma (Sigma-Aldrich, St. Louis, MO, USA), sucrose (Sigma-Aldrich), ethanol (Macklin), glycine (Sigma-Aldrich), hydrochloric acid (Macklin), perchloric acid (Sigma-Aldrich), 3-(4-morpholino)propanesulfonic acid (MOPS, Solarbio Science & Technology, Beijing, China) and bovine serum albumin (BSA, Sigma-Aldrich) were all used as received.

Recombinant human carcinoembryonic antigen-related cell adhesion molecule 5 (CEA, 130 kDa, C520714), recombinant mouse programmed cell death 1 ligand 1 (PD-L1, 43 kDa, C521652) and anti-CD274 rabbit polyclonal antibody (anti–PD-L1, 150 kDa, D264446) were purchased from Sangon Biotech (Shanghai, China). A 5′-mercapto-modified DNA aptamer specific to sPD-L1 [13], whose sequence is 5′-SH-C6-ACG GGC CAC ATC AAC TCA TTG ATA GAC AAT GCG TCC ACT GCC CGT-3′, was synthesized by Sangon Biotech (Shanghai, China). Ultrapure water from a Millipore water purification system (18.2 MΩ cm) was used in all experiments. All bioaffinity measurements using SPR were performed in 1× phosphate-buffered saline (PBS) solution ([−] $CaCl_2$, [−] $MgCl_2$, pH 7.2–7.4, Crgent

Biotech, Hangzhou, China). All binding measurements and the fabrication of aptamers and anti–PD-L1 chips were performed at room temperature or as otherwise specified.

2.2. Preparation of AuNPs-Ab

Gold nanoparticles (AuNPs) with good monodispersity, spherical shape and narrow size distribution are easy to prepare and modify, and AuNPs (20 nm) were used in this work. They were synthesized using the citrate reduction of $HAuCl_4 \cdot 3H_2O$ in a one-pot process [14,15].

The conjugation process of AuNPs to antibodies is similar to those outlined in previous studies but with some modifications [16]. AuNPs were modified using carboxy-terminated thiols activated with amino-coupling reagents and encapsulated with anti–PD-L1. The preparation of AuNPs-Ab (AuNPs modified with anti–PD-L1) is described below. To functionalize the AuNPs with carboxy-terminated thiols, the AuNP colloidal solution was centrifuged (10,000 r/min, 10 min) to remove the supernatant and resuspended in ultrapure water at a concentration of 0.33 nM. MUA (333 μM) was then added to the AuNP solution, and the mixture was shaken overnight at room temperature. The unbound MUA was removed via repeated washing: the thiolated AuNP solution was centrifuged (10,000 r/min, 10 min) to remove the supernatant and dissolved in ultrapure water. To covalently attach anti–PD-L1, 250 μL of thiolated AuNPs (0.275 nM) was mixed with 25 μL NHS/EDC solution (3 mM, ratio NHS:EDC = 1:5) for 5 min. The activated thiolated AuNPs were centrifuged (10,000 r/min, 3 min) and redissolved in 250 μL MOPS buffer (1 mM, pH 7.4) with anti–PD-L1 (30 μg/mL), and the solution was shaken overnight at room temperature. Next, the mixture was repeatedly washed (10,000 r/min, 10 min) with ultrapure water to remove unbound proteins and the solution was kept at 4 °C until use.

In order to confirm that the method produced unaggregated AuNPs-Ab, the absorption spectrum of the solution was measured using an ultraviolet–visible spectrophotometer (TU-1901, Persee General Instrument Co., Ltd., Beijing, China).

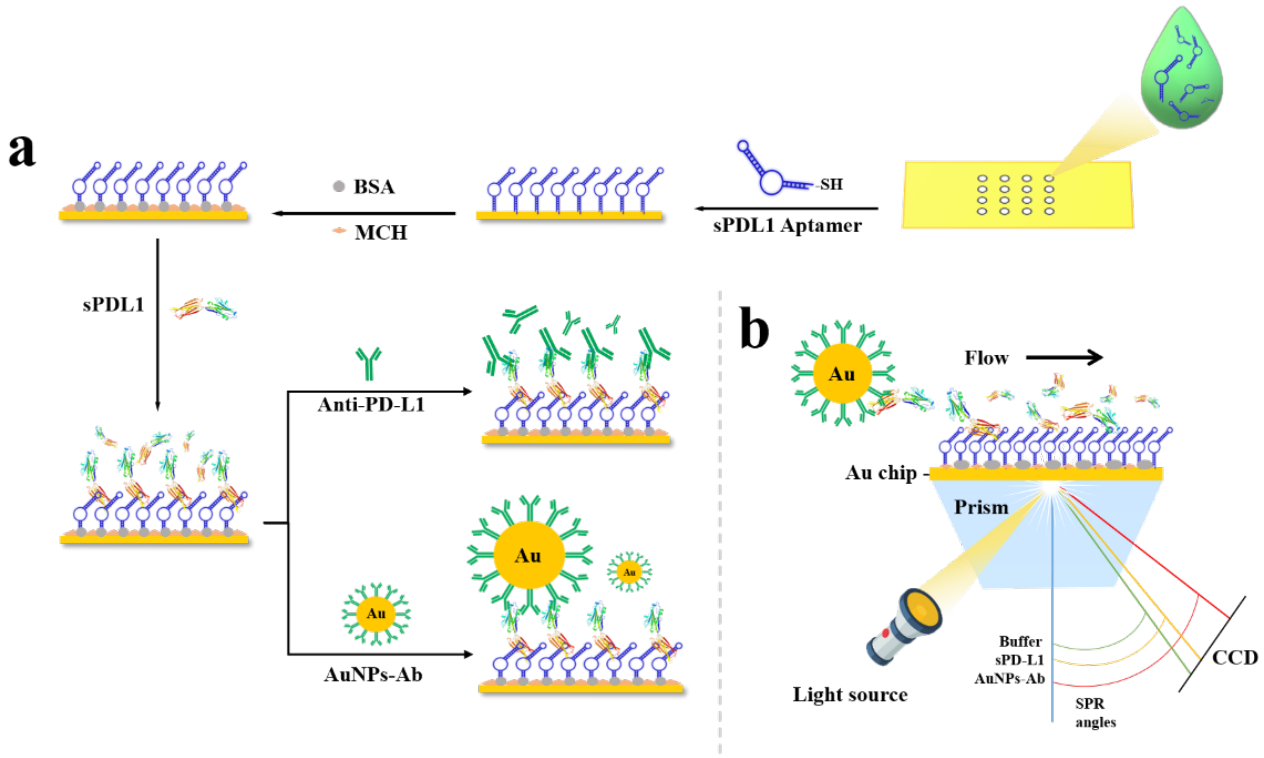
2.3. Creation of Aptamer-Modified SPR Chips

The gold chip (HORIBA Scientific SAS, Palaiseau, France) consists of a high refractive index glass slide covered with a thin gold layer. It was cleaned with ethanol and ultrapure water, respectively, and then dried with nitrogen. The chip was immersed in fresh piranha solution (98% H_2SO_4/H_2O_2, 7:3 (v/v)) at 40 °C for 6 h, then washed thoroughly with ultrapure water and dried in order to obtain a clean surface. A summary of the surface immobilization used for attaching PD-L1 aptamers onto a gold surface is shown in Scheme 1. Briefly, PD-L1 aptamers (c = 1, 2.5, 5, 10 μM) were dissolved in 1× PBS solution and a regular array (2 × 4) was formed on the chip surface using an arrayer. The volume of each point was 0.2 μL and the diameter of each circular point was about 1.5 mm. Next, the chip was exposed to PD-L1 aptamers for a minimum of 24 h in a humidity chamber at 4 °C. After incubation, the chip was rinsed with ultrapure water. Then, the modified surface was covered with 1 mM MCH for 30 min to occupy the blank site of the unbound ligands for the purpose of blocking the chip. Finally, the above cleaning and drying processes were repeated once again. The aptamer-modified chip was kept at room temperature prior to SPRi measurements.

2.4. SPRi Measurements

OpenPleX (version, HORIBA Scientific SAS, Palaiseau, France) was used to monitor the biomolecule binding process. The system and the SPRi chip were stabilized for more than 20 min before each experiment. The area of the point to be read by the CCD was then selected (usually located in the center of the point). The CCD response of each spot was then calibrated and normalized by injecting 200 μL of sucrose 3 mg/mL. All experiments were performed using 1× PBS (pH 7.4) solution as the mobile phase with a flow rate of 10 μL/min (protein) and 50 μL/min (surface regeneration). Different concentrations of sPD-L1 in 1× PBS buffer were injected into the aptamer-functionalized SPR chip for 40 min

to ensure sufficient contact between sPD-L1 and the chip surface aptamers [17]. Chip surface regeneration was achieved through 100 mM Gly-HCl (pH 2).



Scheme 1. Preparation process of sPD-L1 detection platform (**a**) and the schematic diagram of aptamer/sPD-L1/AuNPs-Ab sandwich structure for detection of sPD-L1 (**b**).

For the selection of the optimal concentration of aptamers, a fixed concentration (20 nM) of PD-L1 dissolved in 1× PBS solution was bound to different concentrations of aptamers on the chip surface for 40 min, followed by 10 min of washing with 1× PBS to remove unbound protein and compare the signal response values. The optimal concentration of anti–PD-L1 was chosen by injecting different concentrations of anti–PD-L1 on the surface of the aptamer/sPD-L1 protein complex and analyzing the signal response values. Subsequent experiments were performed using the optimal concentrations of the aptamer as well as anti–PD-L1. For sandwich assays, sPD-L1 was dissolved in 1× PBS solution to form solutions of varying concentrations from 0.05 nM to 10 nM and injected into the sensor chip for SPR analysis. Standard addition was performed for SPR analysis of serum samples [18]. sPD-L1 was dissolved in pre-treated serum to form a 10 nM sample. Using a freshly prepared functionalized chip, the chip surface was first covered by flowing through blank serum for 40 min, washed with 1× PBS solution to obtain a basal signal response value and then injected with a serum sample containing 10 nM sPD-L1. The response value obtained from the measurement needs to be subtracted from the basal signal before analysis. For non-specific binding measurements, 1 nM CEA or AA were injected onto the surface of the chip to test the selectivity of the sensor, and at least three groups of sensors were used for validation. For sensor selectivity and repeatability testing, six sets of sensors prepared under the same conditions were used for the detection of the same concentration of sPD-L1 as well as anti–PD-L1, and the same SPR sensor was regenerated multiple times using 100 mM Gly-HCl (pH 2). The deviation of multiple test response values was calculated.

For AuNP enhancement experiments, a further exploration of the lowest detection limit of sPD-L1, sPD-L1 was dissolved in 1× PBS solution to form solutions of different concentrations from 100 fM to 50 pM and injected into the sensor chip for SPR analysis. Anti–PD-L1 was

replaced with AuNPs-Ab to achieve ultralow-concentration sPD-L1 detection by amplifying the SPR signal through local plasmon resonance effect and mass-loading effect.

3. Results and Discussion

3.1. Optimization of Detection Conditions

The sandwich assay is used for SPR signal amplification, which is based on the principle of increasing the surface mass loading of the chip to obtain a greater change in the refraction angle. As shown in Scheme 1, an SPR-sensing platform based on a sandwich structure formed by aptamer/target protein/antibody was designed to achieve the selective detection of sPD-L1, as both trace and important serums. The SPR was used to monitor the modifications at each step in real time and to validate the response process of the constructed sensor.

Nucleic acid aptamers are small in vitro-screened oligonucleotide sequences or short polypeptides that specifically bind target proteins, peptides or other high-affinity small molecules. Compared to their proteinaceous counterparts (e.g., antibodies), aptamers are more economical, highly specific, have good affinity, are reproducible and can be made more versatile by simple modifications, such as the addition of a sulfhydryl group to the base terminus [19]. It is generally believed that the thiol self-assembled monolayer (SAM) is obtained based on the bonding of the sulfhydryl groups to the inert metal surface atoms and the directional arrangements induced by the physicochemical forces [20]. The immobilization of the aptamer is achieved by coupling the pre-modified base sequence through the strong interaction between the sulfhydryl group and gold, followed by blocking with 1 mM MCH for 30 min to reduce specific binding and allow the aptamer to stand on the surface of the chip [21]. The effect of aptamer immobilization is shown via flow cell images obtained from the real-time monitoring of the chip on the SPRi instrument (Figure 1a). As shown in Figure 1b, a small signal response was observed when trace amounts of sPD-L1 were poured across the gold chip at a certain flow rate, a result that verifies the specific binding between the chosen aptamer and sPD-L1, which is consistent with previous studies [13]. Anti–PD-L1 was then poured over the aptamer/sPD-L1 surface. The specific recognition between the extracellular region of sPD-L1 and anti–PD-L1 resulted in a significant change in signal response, and the results showed that the sandwich method induced a three-fold higher change in SPR signal than the direct detection of sPD-L1. Therefore, the above results indicate that the method has good SPR feasibility and that the constructed sandwich structure formed by the aptamer/sPD-L1/anti–PD-L1 can be used as an effective means of sPD-L1 sensor signal amplification.

There are many parameters that influence the detection process, but the aptamer used to capture sPD-L1 and anti–PD-L1, which enhances the sensitivity during the construction of the sandwich structure, has a greater impact on the detection results. In order to obtain the best experimental results, two experimental conditions were optimized, including the concentration of aptamer and anti–PD-L1. The process of aptamer concentration optimization is as follows. The different concentrations of aptamer (1, 2.5, 5 and 10 μM) were immobilized on the chip surface. When the same concentration of sPD-L1 flows over the chip surface, the SPR signal response process is shown in Figure 2a. The ripple in the middle of the curve is caused by the refractive index of the protein solution that is different to that of the buffer. Three groups of repeated samples were set up for the detection of each aptamer concentration, and the error line was calculated. The response value after signal smoothing is shown in Figure 2b, and the 5 μM aptamer has the largest signal response value as the optimal concentration. Then, 30 nM, 60 nM and 90 nM anti–PD-L1 were sequentially poured on the aptamer/sPD-L1 surface (Figure 2c), and it was found that the SPR angle change gradually increased with improving concentration. After analyzing the stabilized signal values, it was found that the amount of SPR angle change reaches a maximum at 90 nM anti–PD-L1 concentration (Figure 2d), showing the best signal amplification. The optimized process conditions were used for further experiments.

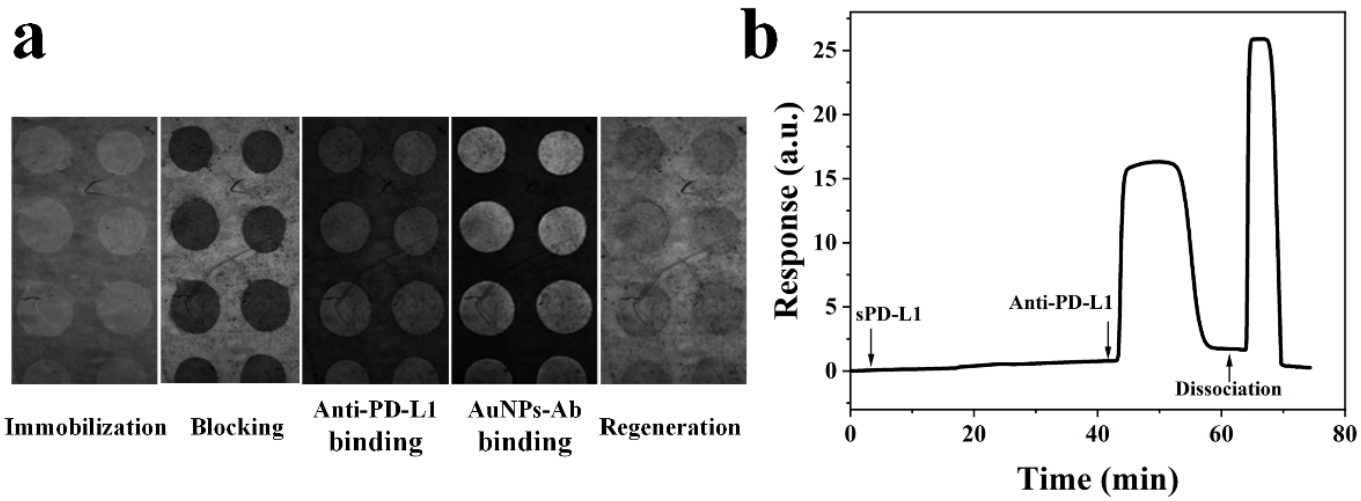


Figure 1. SPRi Chip image of immobilization, blocking, anti-PD-L1 binding, AuNPs-Ab binding and regeneration (**a**). Real-time SPR sensorgram of the step-by-step manufacturing process: specific recognition and binding of injected sPD-L1 and aptamer pre-immobilized on the chip surface, subsequent signal amplification with anti–PD-L1 and, finally, the material dissociation and regeneration on the chip surface using 100 mM Gly-HCl (pH 2) (**b**).

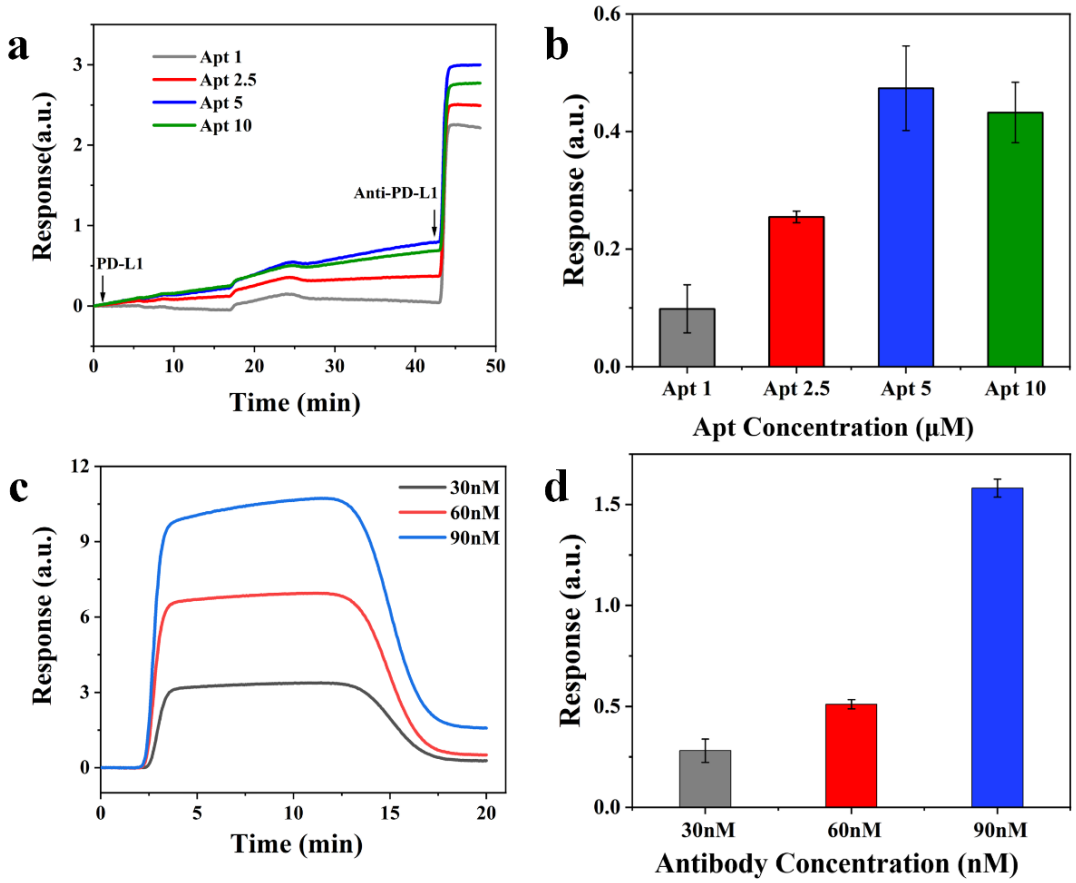


Figure 2. Optimization of aptamer concentration: SPR signal response curves (**a**) for the aptamer-specific (1 μM, 2.5 μM, 5 μM, 10 μM) recognition of 20 nM sPD-L1 and response values (**b**). Optimization of anti–PD-L1 concentration: SPR signal response curves (**c**) for anti–PD-L1 (30 nM, 60 nM, 90 nM), connecting 10 nM sPD-L1 and the response values (**d**).

3.2. Label-Free Detection of sPD-L1

Serum sPD-L1 is a viable biomarker for determining patients' risk-adapted treatment strategies and assessing the probability of recurrence after treatment [22,23]. After the optimization of the main parameters of the constructed sensor, the optimal concentration of aptamer was determined to be 5 μM and the optimal concentration of anti–PD-L1 was 90 nM, based on which the sensitivity of the constructed sensor was measured. Firstly, 5 μM of aptamer was fixed on the chip surface, and the chip was placed into the SPRi platform after using MCH closure. The SPRi chip image of immobilization is shown in Figure 1a. It can be seen that the difference between the pre-fixed aptamer area and the blank area of the chip exists via SPRi (light-colored dots are the aptamer samples, and the rest of the area is the negative control), which proves the successful fixation of the aptamers. Then, 5% BSA was injected for secondary blocking to decrease the specific adsorption on the chip surface further. Usually, the higher the brightness of the chip surface means the greater the change in the SPR refraction angle. Blocking (Figure 1a) shows that the aptamer spots are much darker than the negative control area, indicating that there was no obvious non-specific adsorption between aptamer and BSA, and the selected aptamer has a certain level of selectivity and that secondary closure is necessary.

After the preparation work was completed, the detection of sample sPD-L1 was begun. For the aptamer capture of sPD-L1, the SPR signal response is shown in Figure 1b, the SPR signal response caused by 10 nM sPD-L1 is not obvious and there is no visible difference on the chip surface through the SPRi chip image. After the passage of 90 nM anti–PD-L1 for signal amplification, as shown in Figure 1a (anti–PD-L1 binding), the brightness changes in the aptamers' fixed region and there is a significant change in the SPR signal curve, implying that anti–PD-L1 successfully binds specifically to the sPD-L1 captured by the aptamer and the signal is significantly amplified. The denaturation dissociation of surface proteins and chip surface regeneration (Figure 1a) were used in conjunction with 100 mM Gly-HCl (pH 2) in the process of performing the detection of different concentrations of sPD-L1. Next, the sensor sensitivity was explored by passing the different concentrations of sPD-L1 (0.05–10 nM), and Figure 3a shows that the SPR response values decreased gradually as the concentration of sPD-L1 decreased. The SPR response values after signal stabilization are shown in Figure 3b. The standard deviation was calculated and linear fit analysis showed a good linear relationship between the concentration of sPD-L1 at 0.05–10 nM and the signal response value of the sensor. A linear equation of $y = 0.084x + 0.36$ ($R^2 = 0.9938$) was obtained. In addition, the limit of detection (LOD) was determined to be 0.012 nM at triple its standard deviation from blank measurement. The dual mass loading of aptamers and anti–PD-L1 made the biosensor more sensitive to the change in the refractive angle, thus achieving a good performance enhancement. Since the amount of soluble PD-L1 varies greatly at different stages of cancer progression, the concentration of sPD-L1 in the plasma of patients with advanced lung cancer can be as high as 20 ng/mL [24], and the optimal sPD-L1 threshold for predicting the risk of multiple myeloma (MM) progression is 2.783 ng/mL [25]. Therefore, a large range of sPD-L1 detections is needed to meet the needs of clinical testing. The constructed aptamer/sPD-L1/anti–PD-L1 sensor detects in the range of 0.05–10 nM (2.15–430 ng/mL), which well covers the detection needs of different stages of tumor development and has good applicability in clinical aspects.

3.3. AuNPs-Ab Signal Amplification

The work of Inju Cho et al. predicted primary central nervous system lymphoma (PCNSL) by comparing serum sPD-L1 concentrations in patients (0.429 ng/mL) with healthy controls (0.364 ng/mL) and survival outcome of patients [26]. The diagnosis of colorectal cancer (CRC) via the detection of sPD-L1 has also been covered, with significantly higher sPD-L1 pre-treatment levels in the serum of CRC patients (321.31 ± 55.3 pg/mL) compared to healthy controls (246.78 ± 50.2 pg/mL) [27]. Thus, it is clear that high sensitivity is necessary in clinical applications, and biosensors constructed using only the aptamer/sPD-L1/anti–PD-L1 sandwich method still have limitations. It has been proven

that resonant plasmon coupling between AuNPs and gold thin films can produce large field enhancements and thus improve the SPR [11,28]. In this study, the local plasmon effect between AuNPs and the chip surface is utilized to further enhance the sensitivity of the biosensor (Scheme 1). AuNPs with a diameter of 20 nm were used and modified using anti–PD-L1. The UV–Vis spectra measurements in Figure 4a show the modification effect of AuNPs. The absorption peak of the modified AuNPs (AuNPs-Ab) was shifted from 522 nm to 530 nm, indicating that the antibodies were successfully coupled with AuNPs [29]. The process of detecting sPD-L1 (0.05 nM) was consistent with the above, and in the last step of specific binding, the above anti–PD-L1 was replaced with AuNPs-Ab, and a significant change in brightness at the aptamer spot could be seen via SPRi after the influx of AuNPs-Ab, meaning that apparent change in the refraction angle of the SPR was induced (Figure 4b), and comparing with only the aptamer/sPD-L1/anti–PD-L1 sandwich assay alone, the signal response value reached 5.38 times higher than the latter, implying that the AuNPs-Ab still have considerable potential to amplify the signal.

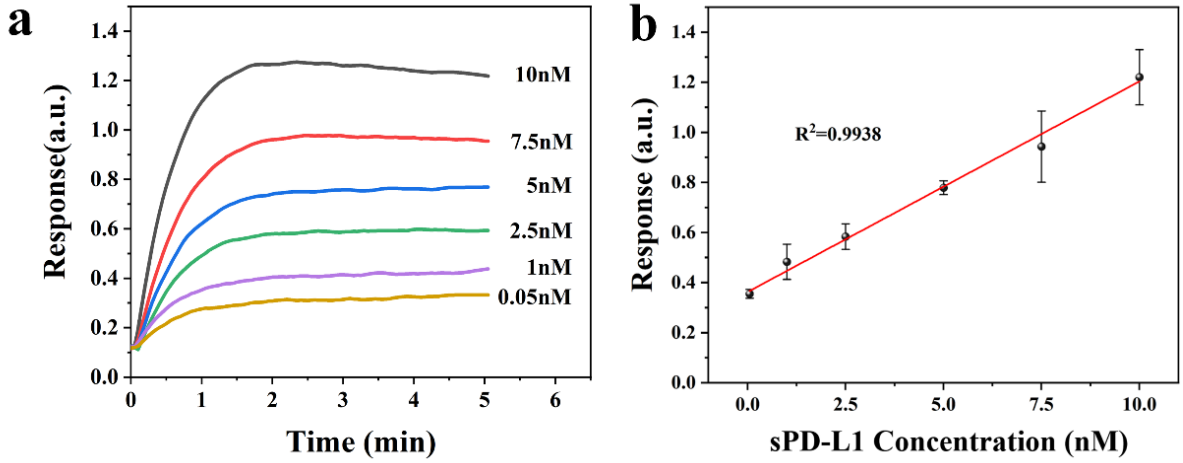


Figure 3. Detection of sPD-L1: the SPR signal response (**a**) caused by the combination of sPD-L1 (0.05–10 nM) and anti–PD-L1 and their corresponding linear relationship (**b**).

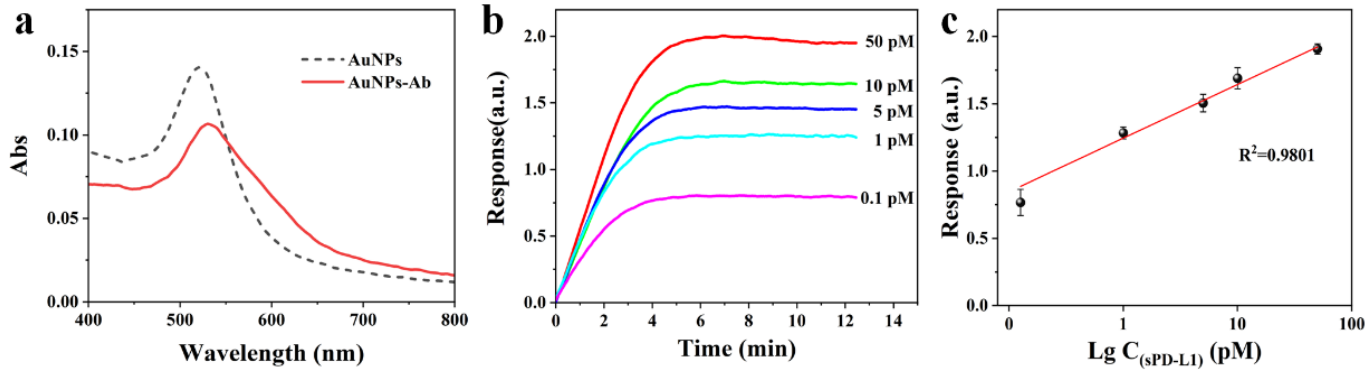


Figure 4. UV–Vis spectra (**a**) of AuNPs (black) and AuNPs-Ab (red). The detection of sPD-L1: the SPR signal response (**b**) caused by the combination of sPD-L1 (100 fM–50 pM) and AuNPs-Ab, and their corresponding linear relationship (**c**).

Then, the detection of lower concentrations of sPD-L1 was tested to further explore the sensitivity. The response curves of SPR signals during the detection process are shown in Figure 4b. With the gradual decrease in the concentration, the intensity of the change in the SPR refraction angle was also seen in the simultaneous weakening. After the SPR signal was stabilized, the standard deviation of the response values at different concentrations was calculated and linearly fitted, and the results are shown in Figure 4c; the concentration of sPD-L1 from 100 fM–50 pM (4.3 pg/mL–2.15 ng/mL) showed a good linear relationship

with the sensor signal response value with the equation $y = 0.85 + 0.39 \times \lg(\text{sPD} - \text{L1})$ (R^2 = 0.9801). The limit of detection (LOD) was determined to be 19 fM at triple its standard deviation from blank measurement. Table S1 (see Supplementary Materials) shows the comparison between the detection of sPD-L1 in this work and in previous works. It is clear that the detection range, linearity relationship and sensitivity are important indicators for evaluating the detection method. The wide detection range facilitates the application of the sensor in multiple scenarios: the precise linearity provides a reference for the quantification of sPD-L1, and the higher sensitivity allows for the more accurate observation of patient status and the assessment of the prognostic probability of recurrence. The constructed sensor has a broader and more practical detection range than other methods (Table S1). The linearity of the relationship is similar to that seen in other works. The very high sensitivity is a remarkable feature of the method, and the relative ease of operation facilitates its application.

3.4. Selectivity and Repeatability of the sPD-L1 Aptasensor

In practical applications, CEA and AA, which are present in serum at the same time as sPD-L1 [30,31], are likely to cause interference during SPRi sensor detection, so CEA and AA were selected as interferents for sensor selectivity testing in this work. The detection method was consistent with that described previously, and at least three groups of sensors were used for validation. Finally, the SPR response values of different substances were compared, and standard deviations were calculated, as shown in Figure 5a, and the change in the SPR refraction angle caused by PD-L1 was significantly more than that of other interfering substances. In order to ensure the rigor of the results, one-way ANOVA was applied to the signal response values of sPD-L1 and CEA and AA, and p was chosen to be 99% and was kept constant during confidence interval comparisons. The results showed that at the 0.01 level, the population means are significantly different ($p < 0.01$). This indicates that the high specificity of sPD-L1 capture was achieved through the dual specific binding of anti–PD-L1, aptamer and sPD-L1, and the constructed sensor has good selectivity.

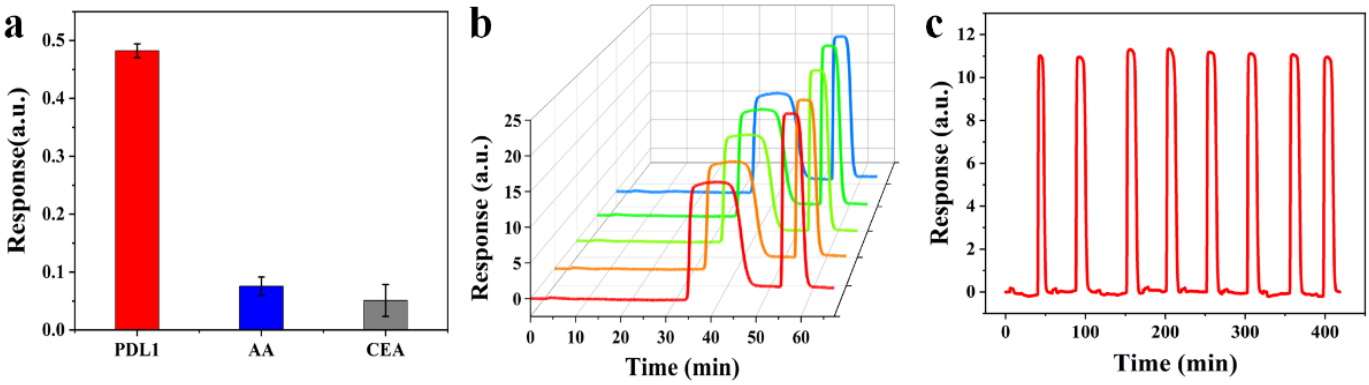


Figure 5. Selectivity of SPRi sensor: 1 nM sPD-L1 caused a greater change in the SPR refractive index than other interfering substances (1 nM CEA or AA), $p < 0.01$ (**a**). Repeatability of SPRi sensor: five sets of sensors prepared under the same conditions were used for the detection (**b**), and an SPRi sensor surface was regenerated multiple times by 100 mM Gly-HCl (pH 2) (**c**).

Moreover, reproducibility is also an essential index. Six sets of sensors prepared under the same conditions were used for the detection of the same concentration of sPD-L1 as well as anti–PD-L1 (Figure 5b), and the relative standard deviation (RSD) of the SPR response values between the five groups of sensors for the same substances was calculated to be 2.06% after signal stabilization, indicating that the operation of the constructed method is reproducible. Afterwards, the same SPR sensor was regenerated multiple times using 100 mM Gly-HCl (pH 2). As shown in Figure 5c, the SPR refraction angle changed steadily without significant differences during the detection process, indicating that the method has good reproducibility.

3.5. Analytical Serum Samples

Clinical detection of sPD-L1 is mostly through the analysis of serum samples. The spiked serum samples were detected using the aptamer/sPD-L1/anti–PD-L1 SPRi sensor and evaluated the feasibility of the sensor. To avoid matrix effects on the assay results, the serum was pre-treated as follows. The plasma and perchloric acid were fully mixed at a proportion of 1:1 and centrifuged for 15 min at 4 °C at a speed of 10,000 r/min. The supernatant was extracted as serum. The serum was diluted to 10% with 1× PBS solution and then used in the SPRi labeling test. sPD-L1 was added at a concentration of 10 nM to test the practical feasibility of the constructed sensor in different environments. Then, 10 nM sPD-L1 dissolved in PBS and spiked serum solution containing 10 nM sPD-L1 were individually injected onto the surface of the aptamer-modified chip. Due to the electrostatic adsorption of proteins from human serum samples to the chip surface and non-specific binding to DNA aptamers, this would result in reduced subsequent capture of anti–PD-L1 on the chip surface and diminished SPR signal. The response curve of SPRi sensor signal after subtracting the background signal caused by blank serum is shown in Figure 6a. It can be seen that the serum environment caused some interference in the detection of sPD-L1, and there may still be non-specific adsorption on the chip surface. The response value after stabilization is also shown in the histogram (Figure 6b). The detection rate of sPD-L1 at the same concentration was still 76.95% under serum conditions compared to the buffer environment. Although the clinical conditions are still to be reached, the results show that the designed sensor is able to accurately and sensitively measure sPD-L1 in serum through the strong specificity between PD-L1 aptamers, anti–PD-L1 and sPD-L1. It means that SPRi sensor has great potential in serum sample analysis, which provides the possibility for the subsequent establishment of efficient methods for clinical analysis. However, the concentration of sPD-L1 is lower in clinical samples. Clinical conditions are still to be reached even if the matrix effect of serum has been used as a starting point. In the future work, we will further explore the effect of changes in relevant experimental conditions on detection.

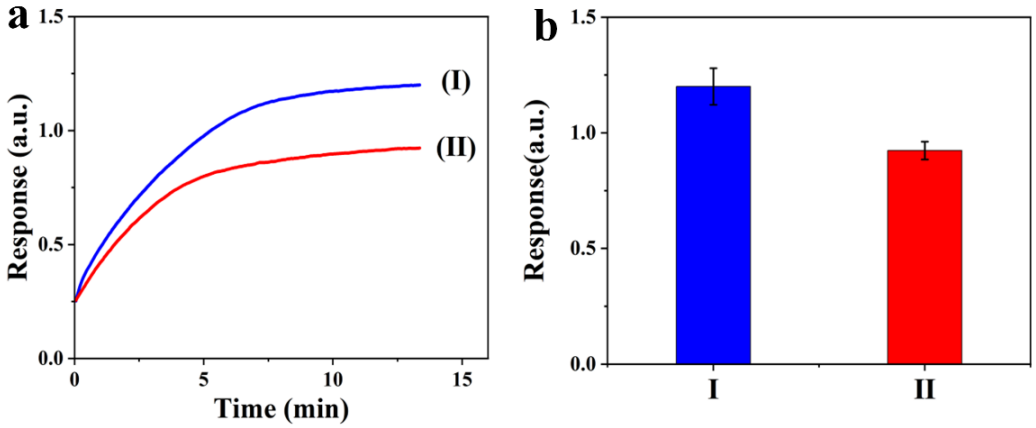


Figure 6. The SPR sensorgram (**a**) and corresponding signal value (**b**) caused by 10 nM sPD-L1 in buffer (I) or human serum samples (II).

4. Conclusions

In summary, an enzyme-free, label-free SPRi sensor based on an aptamer/sPD-L1/anti–PD-L1 sandwich structure was designed and achieved ultrasensitive quantitative measurement of soluble PD-L1 via the signal enhancement with AuNPs. Through the dual loading of the anti–PD-L1 and the aptamer on sPD-L1, the sensor achieved the highly sensitive detection of sPD-L1. sPD-L1 concentration at 0.05–10 nM showed a good linear relationship with the signal response value of the sensor with a linear equation of $y = 0.084x + 0.36$ (R^2 = 0.9938) and a lower limit of detection of 0.012 nM. Further amplification of the SPR sensor surface signal was achieved using the electromagnetic coupling that existed between the SPR of the metal sensing membrane and the localized surface plasmon resonance (LSPR)

of the captured nanoparticles. The coupling of anti–PD-L1 and AuNPs successfully resulted in a 5.38-fold amplification of the SPR signal response, a successful increase in sensitivity by two orders of magnitude, a low detection limit of 19 fM and a good linear relationship between the concentration of sPD-L1 from 100 fM–50 pM and the sensor signal response value with the equation $y = 0.85 + 0.39 \times \lg(\mathrm{sPD-L1})$ (R^2 = 0.9801). The constructed SPRi sensor also has good selectivity as well as reproducibility. The assay of serum samples shows that the sensor has the potential to accurately and sensitively measure sPD-L1 in serum samples. The aptamer/sPD-L1/anti–PD-L1 SPRi sensor designed in this study has the advantages of dynamic monitoring, high sensitivity, easy operation and flexible application scenarios and has excellent potential for using sPD-L1 as a biomarker in the ultrahigh-sensitivity detection of sPD-L1, providing a reference for determining patients' risk-adapted treatment strategies and assessing the probability of recurrence after treatment.

Supplementary Materials: The following are available online at https://www.mdpi.com/article/10.3390/coatings13081400/s1, Table S1: Comparisons of the constructed biosensor with other previous work. References [32–34] are cited in the Supplementary Materials.

Author Contributions: Conceptualization, Y.P., L.J. and X.Y.; methodology, Y.P.; reagent preparation, Y.P. and Y.L.; validation, Y.P.; formal analysis: Y.P. and Y.L.; writing—original draft preparation, Y.P. and Y.L.; writing—review and editing, L.J. and X.Y.; supervision, L.J. and X.Y. All authors have read and agreed to the published version of the manuscript.

Funding: This research was funded by Natural Science Foundation of Zhejiang Province under grant no. LZ22F050004.

Institutional Review Board Statement: Not applicable.

Informed Consent Statement: Not applicable.

Data Availability Statement: Not applicable.

Conflicts of Interest: The authors declare no conflict of interest.

References

1. Ettinger, D.S.; Wood, D.E.; Aisner, D.L.; Akerley, W.; Bauman, J.R.; Bharat, A.; Bruno, D.S.; Chang, J.Y.; Chirieac, L.R.; D'Amico, T.A. Non–small cell lung cancer, version 3.2022, NCCN clinical practice guidelines in oncology. *J. Natl. Compr. Cancer Netw.* **2022**, *20*, 497–530. [CrossRef] [PubMed]
2. Daassi, D.; Mahoney, K.M.; Freeman, G.J. The importance of exosomal PDL1 in tumour immune evasion. *Nat. Rev. Immunol.* **2020**, *20*, 209–215. [CrossRef] [PubMed]
3. Shigemori, T.; Toiyama, Y.; Okugawa, Y.; Yamamoto, A.; Yin, C.; Narumi, A.; Ichikawa, T.; Ide, S.; Shimura, T.; Fujikawa, H. Soluble PD-L1 Expression in Circulation as a Predictive Marker for Recurrence and Prognosis in Gastric Cancer: Direct Comparison of the Clinical Burden Between Tissue and Serum PD-L1 Expression. *Ann. Surg. Oncol.* **2019**, *26*, 876–883. [CrossRef]
4. Shen, H.; Ji, Y.; Zhou, D.; Zhang, Y.; Wang, W.; Sun, J.; Zhang, W. Soluble programmed death-ligand 1 are highly expressed in peripheral T-cell lymphoma: A biomarker for prognosis. *Hematology* **2019**, *24*, 392–398. [CrossRef] [PubMed]
5. Jalali, S.; Price-Troska, T.; Paludo, J.; Villasboas, J.; Kim, H.-J.; Yang, Z.-Z.; Novak, A.J.; Ansell, S.M. Soluble PD-1 ligands regulate T-cell function in Waldenstrom macroglobulinemia. *Blood Adv.* **2018**, *2*, 1985–1997. [CrossRef]
6. Wei, W.; Xu, B.; Wang, Y.; Wu, C.; Jiang, J.; Wu, C. Prognostic significance of circulating soluble programmed death ligand-1 in patients with solid tumors. *Medicine* **2018**, *97*, e9617. [CrossRef]
7. Hu, J.; Zhang, Z.H.; Zhu, Z.; Chen, J.; Hu, X.; Chen, H. Specific intracellular binding peptide as sPD-L1 antibody mimic: Robust binding capacity and intracellular region specific modulation upon applied to sensing research. *Biosens. Bioelectron.* **2021**, *185*, 113269. [CrossRef]
8. Takeuchi, M.; Doi, T.; Obayashi, K.; Hirai, A.; Iwai, Y. Soluble PD-L1 with PD-1-binding capacity exists in the plasma of patients with non-small cell lung cancer. *Immunol. Lett.* **2018**, *196*, 155–160. [CrossRef]
9. Xing, Y.; Liu, J.; Sun, S.; Ming, T.; Cai, X. New electrochemical method for programmed death-ligand 1 detection based on a paper-based microfluidic aptasensor. *Bioelectrochemistry* **2021**, *140*, 107789. [CrossRef]
10. Nguyen, H.H.; Park, J.; Kang, S.; Kim, M. Surface Plasmon Resonance: A Versatile Technique for Biosensor Applications. *Sensors* **2015**, *15*, 10481–10510. [CrossRef]
11. Yang, C.T.; Wu, L.; Bai, P.; Thierry, B. Investigation of plasmonic signal enhancement based on long range surface plasmon resonance with gold nanoparticle tags. *J. Mater. Chem. C* **2016**, *4*, 9897–9904. [CrossRef]

12. Wu, P.F.; Fan, X.Y.; Xi, H.Y.; Pan, N.; Shi, Z.Q.; You, T.T.; Gao, Y.K.; Yin, P.G. Multifunctional self-assembled gold nanorod monolayer/$Ti_3C_2T_x$ nanocomposites based on interfacial electrostatic for highly sensitive SERS detection of organic dyes and adenine. *J. Alloys Compd.* **2022**, *920*, 165978. [CrossRef]
13. Zhang, D.; Zheng, Y.; Lin, Z.; Liu, X.; Li, J.; Yang, H.; Tan, W. Equipping Natural Killer Cells with Specific Targeting and Checkpoint Blocking Aptamers for Enhanced Adoptive Immunotherapy in Solid Tumors. *Angew. Chem. Int. Ed.* **2020**, *59*, 12022–12028. [CrossRef] [PubMed]
14. Elahi, N.; Kamali, M.; Baghersad, M.H. Recent biomedical applications of gold nanoparticles: A review. *Talanta* **2018**, *184*, 537–556. [CrossRef] [PubMed]
15. Lin, X.; Fang, G.; Liu, Y.; He, Y.; Dong, B. Marangoni Effect-Driven Transfer and Compression at Three-Phase Interfaces for Highly Reproducible Nanoparticle Monolayers. *J. Phys. Chem. Lett.* **2020**, *11*, 3573–3581. [CrossRef]
16. Springer, T.; Chadtova Song, X.; Ermini, M.L.; Lamacova, J.; Homola, J. Functional gold nanoparticles for optical affinity biosensing. *Anal. Bioanal. Chem.* **2017**, *409*, 4087–4097. [CrossRef]
17. Lee, S.H.; Park, Y.E.; Lee, J.E.; Lee, H.J. A surface plasmon resonance biosensor in conjunction with a DNA aptamer-antibody bioreceptor pair for heterogeneous nuclear ribonucleoprotein A1 concentrations in colorectal cancer plasma solutions. *Biosens. Bioelectron* **2020**, *154*, 112065. [CrossRef]
18. Gogola, J.L.; Martins, G.; Gevaerd, A.; Blanes, L.; Cardoso, J.; Marchini, F.K.; Banks, C.E.; Bergamini, M.F.; Marcolino-Junior, L.H. Label-free aptasensor for p24-HIV protein detection based on graphene quantum dots as an electrochemical signal amplifier. *Anal. Chim. Acta* **2021**, *1166*, 338548. [CrossRef]
19. Maimaitiyiming, Y.; Hong, F.; Yang, C.; Naranmandura, H. Novel insights into the role of aptamers in the fight against cancer. *J. Cancer Res. Clin. Oncol.* **2019**, *145*, 797–810. [CrossRef]
20. Inkpen, M.S.; Liu, Z.F.; Li, H.; Campos, L.M.; Neaton, J.B.; Venkataraman, L. Non-chemisorbed gold-sulfur binding prevails in self-assembled monolayers. *Nat. Chem.* **2019**, *11*, 351–358. [CrossRef]
21. Manera, M.; Spadavecchia, J.; Leone, A.; Quaranta, F.; Rella, R.; Dellatti, D.; Minunni, M.; Mascini, M.; Siciliano, P. Surface plasmon resonance imaging technique for nucleic acid detection. *Sens. Actuators B* **2008**, *130*, 82–87. [CrossRef]
22. Zhou, J.; Mahoney, K.M.; Giobbie-Hurder, A.; Zhao, F.; Lee, S.; Liao, X.; Rodig, S.; Li, J.; Wu, X.; Butterfield, L.H.; et al. Soluble PD-L1 as a Biomarker in Malignant Melanoma Treated with Checkpoint Blockade. *Cancer Immunol. Res.* **2017**, *5*, 480–492. [CrossRef] [PubMed]
23. Bailly, C.; Thuru, X.; Quesnel, B. Soluble Programmed Death Ligand-1 (sPD-L1): A Pool of Circulating Proteins Implicated in Health and Diseases. *Cancers* **2021**, *13*, 3034. [CrossRef]
24. Okuma, Y.; Hosomi, Y.; Nakahara, Y.; Watanabe, K.; Sagawa, Y.; Homma, S. High plasma levels of soluble programmed cell death ligand 1 are prognostic for reduced survival in advanced lung cancer. *Lung Cancer* **2017**, *104*, 1–6. [CrossRef]
25. Wang, L.; Wang, H.; Chen, H.; Wang, W.D.; Chen, X.Q.; Geng, Q.R.; Xia, Z.J.; Lu, Y. Serum levels of soluble programmed death ligand 1 predict treatment response and progression free survival in multiple myeloma. *Oncotarget* **2015**, *6*, 41228–41236. [CrossRef] [PubMed]
26. Cho, I.; Lee, H.; Yoon, S.E.; Ryu, K.J.; Ko, Y.H.; Kim, W.S.; Kim, S.J. Serum levels of soluble programmed death-ligand 1 (sPD-L1) in patients with primary central nervous system diffuse large B-cell lymphoma. *BMC Cancer* **2020**, *20*, 120. [CrossRef] [PubMed]
27. Shao, W.; Xu, Y.; Lin, S.; Gao, J.; Gao, J.; Wang, H. The potential of soluble programmed death-ligand 1 (sPD-L1) as a diagnosis marker for colorectal cancer. *Front. Oncol.* **2022**, *12*, 988567. [CrossRef]
28. Fathi, F.; Rashidi, M.-R.; Omidi, Y. Ultra-sensitive detection by metal nanoparticles-mediated enhanced SPR biosensors. *Talanta* **2019**, *192*, 118–127. [CrossRef]
29. Okyem, S.; Awotunde, O.; Ogunlusi, T.; Riley, M.B.; Driskell, J.D. Probing the Mechanism of Antibody-Triggered Aggregation of Gold Nanoparticles. *Langmuir* **2021**, *37*, 2993–3000. [CrossRef]
30. Wang, W.; Xu, X.; Tian, B.; Wang, Y.; Du, L.; Sun, T.; Shi, Y.; Zhao, X.; Jing, J. The diagnostic value of serum tumor markers CEA, CA19-9, CA125, CA15-3, and TPS in metastatic breast cancer. *Clin. Chim. Acta* **2017**, *470*, 51–55. [CrossRef]
31. Kashiouris, M.G.; L'Heureux, M.; Cable, C.A.; Fisher, B.J.; Leichtle, S.W.; Fowler, A.A. The Emerging Role of Vitamin C as a Treatment for Sepsis. *Nutrients* **2020**, *12*, 292. [CrossRef] [PubMed]
32. Moazzam, P.; Myekhlai, M.; Alinezhad, A.; Alshawawreh, F.A.; Bakthavathsalam, P.; Goncales, V.R.; Tilley, R.D.; Gooding, J.J. Ultrasensitive detection of programmed death-ligand 1 (PD-L1) in whole blood using dispersible electrodes. *Chem. Commun.* **2021**, *57*, 2559–2562. [CrossRef] [PubMed]
33. Hu, H.; Ding, Y.; Gao, Z.; Li, H. S1 nuclease digestion-based rational truncation of PD-L1 aptamer and establishment of a signal dual amplification aptasensor. *Sens. Actuators B* **2021**, *331*, 129442. [CrossRef]
34. Mao, Z.; Zhu, H.; Peng, X.; Chen, J.; Chen, Q.; Chen, X.; Hu, X.; Chen, H. In situ vertical alignment of 2D MoS(2) layers on GO film: Enhanced electrochemical properties for PD-L1 sensing. *Microchim. Acta* **2022**, *189*, 155. [CrossRef] [PubMed]

Disclaimer/Publisher's Note: The statements, opinions and data contained in all publications are solely those of the individual author(s) and contributor(s) and not of MDPI and/or the editor(s). MDPI and/or the editor(s) disclaim responsibility for any injury to people or property resulting from any ideas, methods, instructions or products referred to in the content.